Journal of Zhejiang University-SCIENCE A (Applied Physics & Engineering)
ISSN 1673-565X (Print); ISSN 1862-1775 (Online)
www.jzus.zju.edu.cn; www.springerlink.com
E-mail: jzus@zju.edu.cn

Experimental and numerical investigation of flow forces in a seat valve using a damping sleeve with orifices*

Jun-hui ZHANG[1], Di WANG[1], Bing XU[†‡1], Min-yao GAN[2], Min PAN[3], Hua-yong YANG[1]
[1]*State Key Laboratory of Fluid Power and Mechatronic Systems, Zhejiang University, Hangzhou 310027, China*
[2]*Shanghai Marine Equipment Research Institute, Shanghai 200031, China*
[3]*Department of Mechanical Engineering, University of Bath, Bath BA2 7AY, UK*
[†]E-mail: bxu@zju.edu.cn

Received Mar. 29, 2017; Revision accepted Sept. 4, 2017; Crosschecked May 9, 2018

Abstract: The power of hydraulic piston engines is much affected by the on-off valves which control the fuel injection of the piston assembly. Therefore, the opening time of the seat valve used as the on-off valve is optimized by minimizing the axial flow forces on the spool. A damping sleeve with orifices is proposed to change the valve internal geometry. Experimental and numerical investigations of the flow forces acting on the spool with and without the proposed damping sleeve are carried out to identify the differences in the flow field and to minimize the forces' effect. The simulated results fit the experimental results well. Both results show that the proposed damping sleeve affects the pressure distribution along the spool cone surface and the jet stream direction significantly. The effects of the orifice's width, height, and relative sleeve installation positions on the flow field and cavitation are assessed using simulation methods. As a result of the flow field changing, the damping sleeve can reduce the flow forces significantly and even reverse the forces' direction at the cost of a little flow loss. The opening time of the seat valve can be reduced by 31% to 0.67 ms by using the proposed damping sleeve.

Key words: Seat valve; Damping sleeve; Flow forces; Numerical investigation; Cavitation; Hydraulic piston engine
https://doi.org/10.1631/jzus.A1700164 **CLC number:** TH137.523

1 Introduction

The hydraulic free piston engine is a combination of a combustion engine and hydraulic linear pumps. It has the advantages over the conventional engine of lower maintenance costs and less energy consumption. The operational frequency and the engine power are highly affected by the response time of the on-off valves which control the oil in the fuel injection process (Li et al., 2014, 2015; Zhang et al., 2016). The seat valves are often used as on-off valves since a relatively small movement of the spool can open up a large orifice area (Johnston et al., 1991).

However, the flow forces and the elastic force exerted by the spring act against the driving force and obstruct the spool movement. The flow forces can be so high in high-pressure and large-flow situations that the driving forces need to be redesigned, because the overweighed flow forces reduce the valve opening and slow down the response (Amirante et al., 2014a).

To gain high dynamics, much effort is paid to reduce the steady flow forces by redesigning the flow path through adding some special structures or optimization of the structural parameters (Cheng et al., 2017). The optimization can be distinguished into

---

[‡] Corresponding author

[*] Project supported by the NSFC-Zhejiang Joint Fund for the Integration of Industrialization and Informatization (No. U1509204), China, the National Natural Science Foundation of China (Nos. 91748210 and 51375431), and the Strengthening Industrial Base Project (No. TC150B5C0-29), China

ORCID: Jun-hui ZHANG, https://orcid.org/0000-0002-2603-2065; Bing XU, https://orcid.org/0000-0003-0236-7896 three main approaches: radial flow compensation, jet guiding compensation, and pressure drop compensation (Reichert, 2010), as shown in Fig. 1.

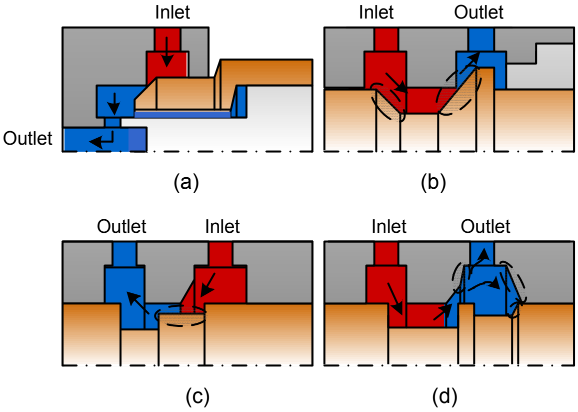

Fig. 1 Different flow forces compensation approaches for seat valves

(a) Radial flow compensation; (b) Spool jet guiding compensation; (c) Pressure drop compensation; (d) Housing jet guiding compensation

The radial flow compensation approach can reduce the flow forces in the axial direction by increasing the jet angle to 90° (Fig. 1a) through circumferential holes. In this way the cosinoidal factor in the calculation can be decreased. Complex and costly design is required by this approach. The jet guiding compensation approach includes shape optimization of the spool (Fig. 1b) and the housing (Fig. 1d). The jet angles at the inlet and outlet control edges are both changed by the inclined surfaces to generate compensating flow forces, as shown in Fig. 1b. In Fig. 1d, the jet angle is changed at the outlet control edge by the flow impingement on the house surfaces to recirculate the flow. The relevant surfaces are spotted using grey ellipses in Fig. 1d. Because of the manufacturing difficulty in the inner contour of the housing, spool jet compensation is preferred in these two compensation approaches (Borghi et al., 2000, 2004; Aung et al., 2015). By optimizing the parameters such as the inlet angle, socket length, and housing gap, the flow forces can be reduced (Simic and Herakovic, 2015). The limitation of the jet guiding approach is that the resultant flow forces cannot be reduced to zero. The pressure drop compensation approach increases the pressure drop at the orifice by an additional resistance (Fig. 1c) near the control edge. The enlarged pressure drop acts on the spool and compensates the steady flow forces. The validity of the pressure drop approach only appears in large flow applications (Merritt, 1967).

Analytical, numerical, and experimental studies have been made to validate the effectiveness of the above compensation methods. Analytical approaches are proposed based on the development of mathematical algorithms to reduce the flow forces (Bergada and Watton, 2004). Numerical methods with the aid of commercial software such as ANSYS Fluent and CFX are also used. Two-dimensional (2D) simulation methods are used to save calculation effort when the axial symmetric fluid models can describe the real condition well enough (Amirante et al., 2006; Beune et al., 2012; Saha et al., 2014). Three-dimensional (3D) models are compared with 2D ones and are found to be better in the study of detailed flow structures (Chattopadhyay et al., 2012). Therefore, 3D models are created to give detailed simulated results of the complex asymmetrical fluid models inside the valve chambers. Experiments are carried out to validate the simulation models as well as the effectiveness of the optimization (Jin et al., 2013; Amirante et al., 2014b; Benzon et al., 2015).

In this paper, a damping sleeve with orifices is designed to reduce the steady axial flow forces in the seat valve. The shapes of the spool and the housing can remain unchanged when the damping sleeve is installed compared with the previous methods, so it can easily be implemented in application. The flow forces can be reduced to zero with proper optimization and the flow loss can be controlled within 5%. The remainder of the paper is structured as follows. The basic principles of this method are provided first. Then, the computational fluid dynamics (CFD) model is established using the ANSYS Fluent turbulence model and a cavitation model. Moreover, a special flow force test rig is designed. At last, the simulated and experimental results of flow forces and flow loss, as well as the discussion, are presented.

2 Flow forces and damping sleeve

2.1 Flow forces in the seat valves

Flow forces refer to the forces which act on the valve spool as a result of fluid flowing in the chambers and through the orifices. Fig. 2 shows the sketch of a given direct-control seat valve. The spool is moved by the solenoid and the spring. The solenoid develops an actuation force (F_{act}) to open the valve. When the valve is opened, the actuation force counteracts the disturbance forces (Simic and Herakovic, 2015) and the elastic force which is exerted by the spring (F_{spring}) to move the spool. The disturbance forces consist of the friction force (F_{f}), the flow forces (F_{flow}) with steady ($F_{\mathrm{flow.stead}}$) and dynamic parts ($F_{\mathrm{flow.dyn}}$), the pressure forces (F_{pres}), and the inertial forces (F_{a}).

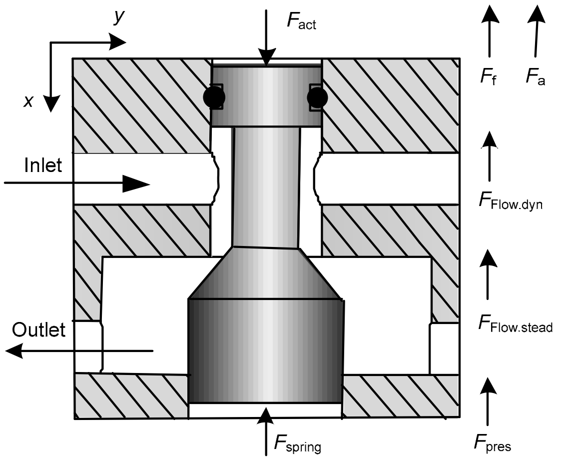

Fig. 2 Forces acting on the spool in a cone-shape seat valve

In this study, we focus on the steady state of the seat valve. Therefore, dynamic parts of disturbance forces are not considered. The inertial forces (F_{a}) and the dynamic flow forces ($F_{\mathrm{flow.dyn}}$), which are caused by the movement of the spool, are not included in the analysis. The friction force (F_{f}) can be divided into the Coulomb friction force (F_{fc}) caused by the radial forces and the viscous friction force (F_{fv}) resulting from the movement of the spool. The viscous friction force (F_{fv}) is also excluded from consideration due to the focus on the steady state. However, the Coulomb friction force (F_{fc}) caused by the O-ring cannot be neglected. To accurately measure the steady flow force ($F_{\mathrm{flow.stead}}$), the stationary part of the Coulomb friction force is removed by the experiments. The targeted test rig is designed and described in Section 4.

2.2 Flow forces reduction method

A flow forces reduction method is proposed in which a damping sleeve is added over the spool, as shown in Fig. 3. The whole valve is composed of the housing, the 1st sleeve, the 2nd sleeve, the spool with the O-ring, and the damping sleeve. The damping sleeve is a socket with four orifices distributed circumferentially, as shown in Fig. 3b. The orifices are designed to be rectangular because of convenient processing. The damping sleeve is fixed by the 1st sleeve and the 2nd sleeve in the axial direction and the spool in the radial direction. A small clearance exists between the spool and the damping sleeve so that the spool can be shifted in the axial direction smoothly.

The fluid first goes into the inlet port on the housing and spreads into the groove on the 1st sleeve. Then the four ports which are evenly distributed along the circumference on the 1st and the 2nd sleeves direct the fluid to the spool. The fluid is impeded by the sleeve wall and throttled by the spool and the sleeve orifices. After that, the fluid goes into the chamber formed by the 1st sleeve and the 2nd sleeve, and finally gets out through the groove on the 1st sleeve and the outlet port.

The emphasis of this method is on changing the structure of the outlet control volume presented in Fig. 3a. Based on published research, this method can be seen as a combination of the pressure drop compensation approach and the jet guiding compensation approach (Reichert, 2010). Analysis of the effects of different damping orifice widths (w shown in Fig. 3b), different orifice heights (h shown in Fig. 3b), and different relative installation positions is made. Four different damping sleeves are manufactured to cover four different orifice widths w (3 mm, 4 mm, 5 mm, and 6 mm). The orifice height of these damping sleeves is chosen to be 2.7 mm so that the orifice bottom surface coincides with the cone edge when the spool moves to its maximum stroke. The effects on the steady flow forces and the flow loss are compared by CFD simulation and experiment. The validity of changing the orifice height h is also analyzed by simulation.

The relative position between the damping orifices and the outlet ports needs to be investigated to establish how it affects the flow structure in the inner chambers. The two limited relative positions of parallel and 45° conditions, as shown in Fig. 4, are analyzed by simulation. The other parameters are chosen to be constants as shown in Fig. 3.

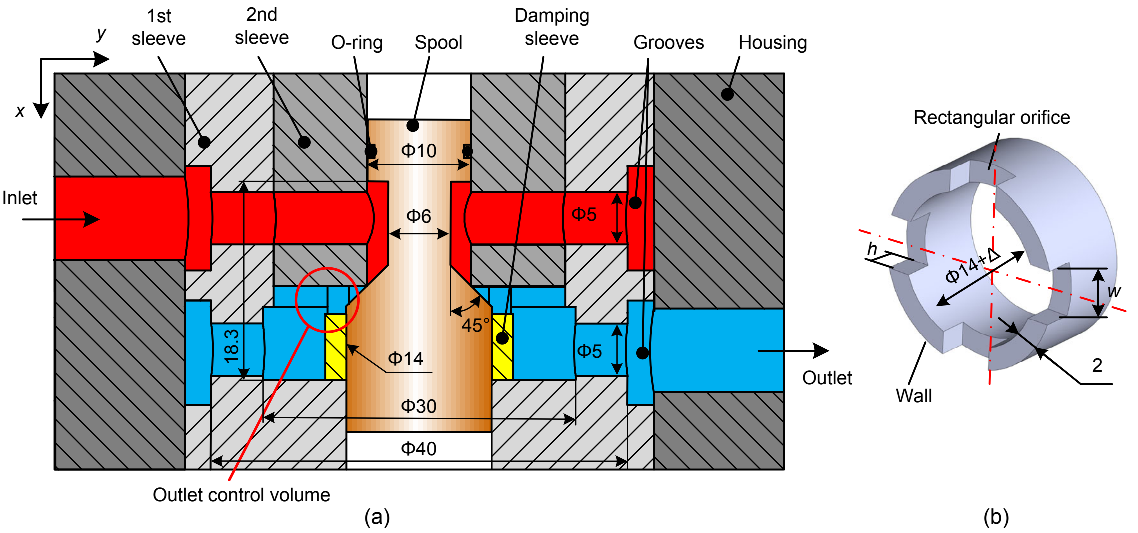

(a) (b)

Fig. 3 Seat valve structure and the proposed damping sleeve (unit: mm)
(a) Structure of the seat valve with damping sleeve; (b) Shape of the damping sleeve

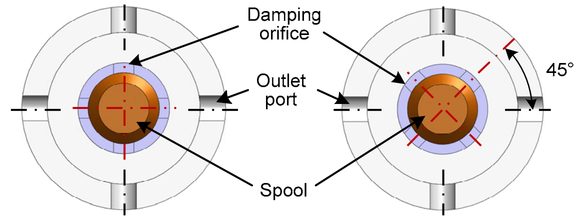

(a) (b)

Fig. 4 Schematic of the relative positions between the damping orifices and the outlet ports
(a) Damping orifices are parallel with outlet ports; (b) Damping orifices are at the angle of 45° to the outlet ports

3 CFD simulation

CFD simulation uses numerical analysis and algorithms to solve a given problem involving fluids. The turbulence which happens in the valve can be described using the Navier-Stokes equations. Direct numerical simulation (DNS) cannot be used because of the limitation of the CPUs in most cases. The Reynolds-averaged Navier-Stokes (RANS) equations were developed to solve the turbulence and simplify the calculation. This calculation can be done using the commercial software, ANSYS Fluent (ANSYS, 2013b). This software provides several different turbulence models including k-ε models and k-ω models. Because of high pressure differential between the inlet and the outlet ports (up to 6 MPa), the flow velocity can be quite high at the throttle opening. From previous studies (Li et al., 2013; Hu et al., 2014; Ji et al., 2017), cavitation occurs in the jet flow. Considering the accuracy and the compatibility with the two-phase cavitation model, the renormalization group (RNG) k-ε model is chosen to describe the turbulence (Valdés et al., 2014; Wu et al., 2015).

The turbulence kinetic energy k, and its dissipation rate ε, can be obtained by

$$\frac{\partial}{\partial t}(\rho k)+\frac{\partial}{\partial x_i}(\rho k u_i)=\frac{\partial}{\partial x_j}\left(\alpha_k \mu_{\text{eff}}\frac{\partial k}{\partial x_j}\right)+G_k+G_{\text{b}}-\rho\varepsilon-Y_{\text{M}}+S_k, \tag{1}$$

$$\frac{\partial}{\partial t}(\rho \varepsilon)+\frac{\partial}{\partial x_i}(\rho \varepsilon u_i)=\frac{\partial}{\partial x_j}\left(\alpha_\varepsilon \mu_{\text{eff}}\frac{\partial \varepsilon}{\partial x_j}\right)+C_{1\varepsilon}\frac{\varepsilon}{k}(G_k+C_{3\varepsilon}G_{\text{b}})-C_{2\varepsilon}\rho\frac{\varepsilon^2}{k}-R_\varepsilon+S_\varepsilon, \tag{2}$$

where t is the time, ρ is the fluid density, and u_i is the mean velocity in the x_i direction. x_i and x_j represent the spatial coordinates in the i- and j-directions, respectively. μ_{eff} is the effective viscosity of fluid, G_k is the generation of turbulence kinetic energy due to mean velocity gradients, G_{b} is the generation of turbulence kinetic energy due to buoyancy, and Y_{M} is the contribution of the fluctuating dilatation in compressible turbulence to the overall dissipation rate. The variables α_k and α_ε indicate the inverse effective Prandtl numbers for k and ε, respectively. S_k and S_ε

denote the user-defined source terms. $C_{1\varepsilon}$, $C_{2\varepsilon}$, and $C_{3\varepsilon}$ are model constants, and R_ε is an addition term for rapid strain and streamline curvature correction (Yakhot and Orszag, 1986; ANSYS, 2013a). The parameters are calculated using the default values provided by ANSYS Fluent.

Cavitation is modeled using the Schnerr and Sauer model. This model follows a similar method as the Singhal et al. model to derive the formula for the net mass transfer from liquid to vapor, but it is more robust and stable than the latter one. This model can be used in all turbulence models (Valdés et al., 2014).

The vapor volume fraction is described by

$$\frac{\partial}{\partial t}\left(\alpha\rho_{\mathrm{v}}\right)+\nabla\cdot\left(\alpha\rho_{\mathrm{v}}\boldsymbol{V}_{\mathrm{v}}\right)=\frac{\rho_{\mathrm{v}}\rho_{\mathrm{l}}}{\rho_{\mathrm{m}}}\frac{\mathrm{d}\alpha}{\mathrm{d}t}. \tag{3}$$

The vapor volume fraction is connected to the bubble number per volume of liquid using

$$\alpha=\frac{n_{\mathrm{b}}\dfrac{4}{3}\pi R_{\mathrm{B}}^{3}}{1+n_{\mathrm{b}}\dfrac{4}{3}\pi R_{\mathrm{B}}^{3}}. \tag{4}$$

The mass transfer rate is derived as

$$R=\frac{\rho_{\mathrm{v}}\rho_{\mathrm{l}}}{\rho_{\mathrm{m}}}\alpha\left(1-\alpha\right)\frac{3}{R_{\mathrm{B}}}\sqrt{\frac{2}{3}\frac{\left(P_{\mathrm{V}}-P\right)}{\rho_{\mathrm{l}}}}, \tag{5}$$

and

$$R_{\mathrm{B}}=\left(\frac{\alpha}{1-\alpha}\frac{3}{4\pi}\frac{1}{n_{\mathrm{b}}}\right)^{\frac{1}{3}}. \tag{6}$$

In Eqs. (3)–(6), α represents the vapor volume fraction, ρ_{v} denotes the vapor density, $\boldsymbol{V}_{\mathrm{v}}$ indicates the vapor phase velocity, and ρ_{l} denotes the liquid phase density. ρ_{m} represents the mixture fluid density, and can be used in Eqs. (1) and (2) as the fluid density. R denotes the mass transfer rate, n_{b} denotes the number of bubbles per volume, R_{B} represents the bubble radius, P_{V} indicates the saturation vapor pressure, and P represents the local far-field pressure.

CFD simulation is applied to validate the effectiveness of the method and to analyze the structure parameters' effects. The purpose is to reduce the axial flow forces while minimizing the flow rate loss.

3.1 Geometry and meshing

Three-dimensional models of the fluid field in the valve are created and presented in Fig. 5. The grooves on the 1st sleeve and the four axisymmetric holes on the 1st and the 2nd sleeves (Fig. 3) are designed to spread the flow evenly into the cone surface. Therefore, the flow field can be seen as symmetric around the spool although there is only one inlet and one outlet port on the housing. In order to simplify the calculation and save time, 1/8 of the flow field is selected based on the symmetry axis and symmetry planes. The simplified flow field is divided into five chambers based on the structure characteristics for better description of the flow and the pressure distribution, as shown in Fig. 5.

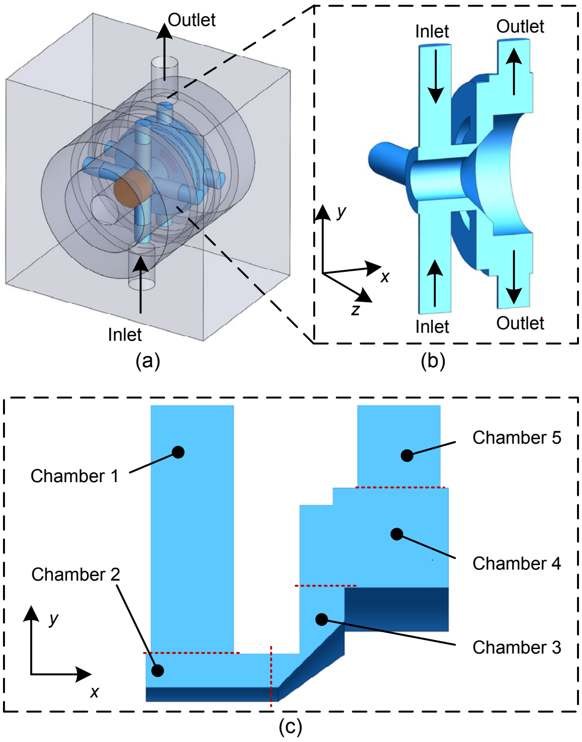

Fig. 5 Schematic of the seat valve and the fluid field
(a) Valve structure; (b) Cross-section of fluid field; (c) 1/8 fluid field

The 3D models are divided into five parts for meshing. The size and the shape of the elements are set differently according to the part shape and the complexity of local flow field. The regular mesh elements (hexahedral) are used to mesh the half-cylinder parts at the inlet and the outlet ports while the irregular mesh elements (tetrahedrons, wedges, or pyramids) are used to mesh the other parts. The most critical region of the metering faces and the cone faces are meshed with the volume element size of 0.1 mm, and a refined meshing is achieved on these faces using the element size of 0.05 mm. The inflation is used on faces with high velocity and strong metering function to get a more accurate near-wall calculation (Shojaeefard et al., 2012). The enhanced wall treatment is selected to model the near-wall flow field. This model combines a two-layer model with the enhanced wall function. It avoids the large computational requirement of the standard wall function and raises the upper limit of non-dimensional distance y^+ requirement from one to ten (ANSYS, 2013b; Martins et al., 2016). Therefore, the first layer thickness of the inflation is set to be 0.03 mm based on the calculation. The generated meshes have around 1.9 million to 2.1 million cells with different damping sleeves. The mesh quality is checked and the aspect ratios are between 18.13 and 36.39. The maximal y^+ calculated by Fluent is reduced to 5.3 through the intentionally refined face meshing.

A grid independence analysis is made before selecting the final mesh size. Simulations on three different models with about 0.9 million, 2.0 million, and 3.3 million cells are performed. The mesh sizes in chamber 3, chamber 4, and chamber 5 (Fig. 5) are especially refined for high speed and possible cavitation. The flow forces are used as the variable to be compared. The simulated and the experimental results are shown in Fig. 6. The results vary little when changing the mesh size. Considering the y^+ requirements for the enhanced wall model, the meshing models with 2.0 million cells are chosen to be simulated. The final generated mesh is shown in Fig. 7.

3.2 Simulation parameters

The simulation parameters, such as material properties and boundary conditions, are set in Fluent and presented in Table 1. The inlet and the outlet pressure are set according to the practical application. The seat valve, in which the damping sleeve is used, is designed for the fuel injection system of the free piston engine and is connected to a hydraulic transformer to compress the fuel. The back pressure of the fuel is zero at the beginning of the compression. The small volume of oil through the valve as well as the relatively large volume in the transformer and the connecting part makes the pressure insensitive during the valve opening. Therefore, the outlet pressure is set to be zero and the inlet pressure is set to the system pressure.

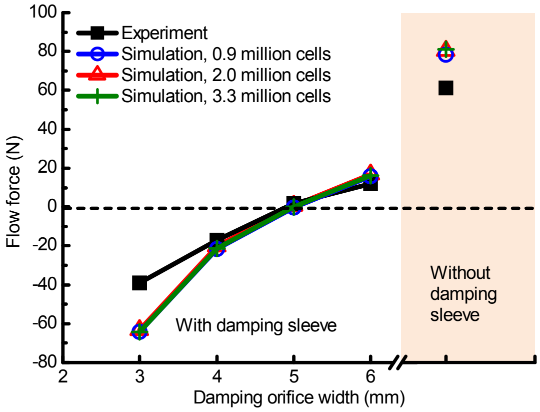

Fig. 6 Flow forces in simulation and experiment

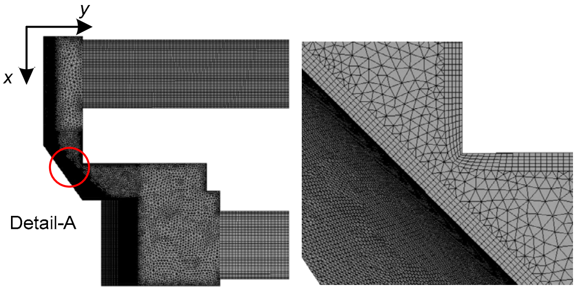

(a) (b)

Fig. 7 3D mesh model
(a) Mesh model; (b) Detail-A

Table 1 Settings of CFD fluid model

Fluid parameter	Boundary condition	Variable parameter
Two-phase flow; mineral oil: ISO VG 46 at 30 °C; density: 850 kg/m^3; dynamic viscosity: 0.068 g/ms; bubble density: 1×10^{14} m^{-3} (Valdés et al., 2014)	Environment pressure: 101 325 Pa (absolute pressure); inlet static pressure: 6 MPa; outlet static pressure: 0; pressure differential: 6 MPa; no slip wall, smooth wall	Damping orifice width: 3–6 mm

4 Test rig for measurement of flow forces

To validate the effectiveness of the damping sleeve for flow forces reduction, experiments are conducted with a specially designed flow forces test rig. The scheme of the flow forces test rig is presented in Fig. 8. The left and the right adjusting screws are used to move the spool from 0 to 0.7 mm and maintain the static position. The exact spool displacement is measured by a micrometer gauge. The pressure in the inlet port is adjusted with the relief valve and the outlet pressure is adjusted with a throttle valve. To simulate the practical condition of the valve, described in Section 3.2, the throttle valve is opened maximally. The return pressure is approximately zero in the experiments considering the disturbance in the signal acquisition system and the pressure sensor accuracy. The flow rate across the valve is monitored by a flow sensor. The main characteristics of the sensors are shown in Table 2.

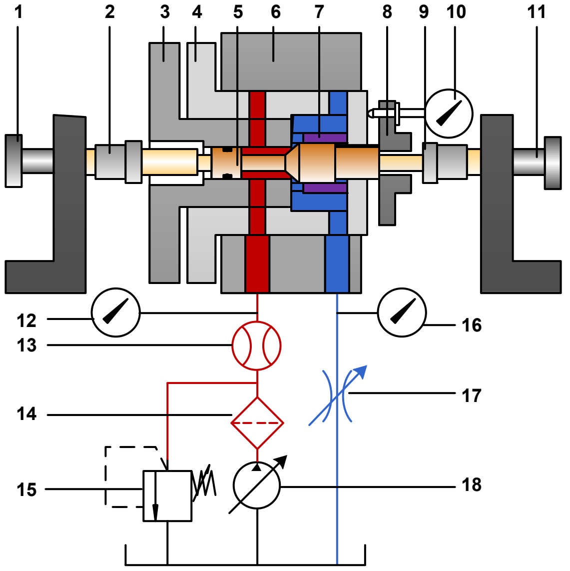

Fig. 8 Schematic of the test rig for the flow forces measurement

1-adjusting screw; 2-force sensor; 3-2nd sleeve; 4-1st sleeve; 5-spool; 6-housing; 7-damping sleeve; 8-mounting block; 9-force sensor; 10-micrometer gauge; 11-adjusting screw; 12-pressure sensor; 13-flow sensor; 14-filter; 15-relief valve; 16-pressure sensor; 17-throttle valve; 18-pump

Since the Coulomb friction force affects measurement accuracy, two force sensors are used to exclude the effect. The tests are first conducted under steady conditions when the valve is opened maximally. The screws are turned until the spool slightly moves and the force data are recorded. Then, the screws are turned in the opposite directions until the spool moves back slightly and the data are recorded. Since the spool movement can be neglected compared to the full stroke, the flow forces are considered to be the same under these two conditions. The only change in the experiments is the direction of the steady friction. Therefore, the flow forces can be calculated with the force data acquired under these two conditions.

Table 2 Main characteristics of the sensors

Sensor	Characteristic
Force sensor	Measuring range: 0–300 N; relative sensitivity error≤±0.1%; temperature sensitivity ≤±0.5% FSO/10K
Pressure sensor	Pressure range: 0–25 MPa; accuracy: ±0.5% FSO; non-linearity≤±0.5% FSO; hysteresis and repeatability≤±0.1% FSO
Flow sensor	Measuring range: 0.05–80 L/min; measurement accuracy: 0.3% FSO; repetition accuracy: ±0.05% FSO; sensitivity: 0.0625 mL/pulse

FSO: full-scale output

5 Results and discussion

For a better understanding of the damping effect, comparisons between the seat valve without the damping sleeve and the seat valve with the damping orifice width of 4 mm are presented in Figs. 9 and 10. The working condition and the flow field affect the pressure distribution and this leads to the pressure forces (F_{pres}) (Fig. 2) acting directly on the spool. The pressure distribution is shown in Fig. 9. The damping effect of the orifices reduces the pressure drop along the spool in the $+x$ direction. The pressure on the part of the cone surface, which corresponds to the wall on the damping sleeve shown in Fig. 3, changes from less than 1 MPa to nearly 2.5 MPa. Therefore, the pressure forces (F_{pres}) in the $-x$ direction can be reduced considerably and thus can be the whole flow forces.

The jet guiding compensation approach is also used in this method. The flow structures are presented in Fig. 10. When the damping sleeve is not installed, the flow is accelerated at the cone surface. Then it impinges on the 1st sleeve (Fig. 3a) and flows back to the spool. It forms swirling vortices in the x direction (Fig. 10a). However, when the damping sleeve is mounted, as shown in Fig. 10b, the stream by the cone surface is first blocked by the damping sleeve wall mentioned in Fig. 3 and forms small vortices near the

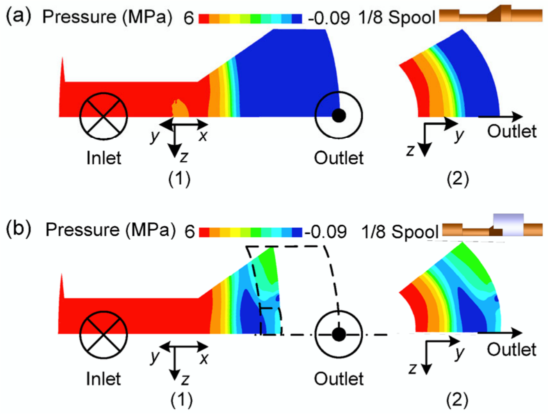

Fig. 9 CFD simulation of pressure distribution on the spool surface

(a) Without damping sleeve: (1) pressure distribution on the spool surface; (2) pressure distribution on the cone surface. (b) With damping sleeve: (1) pressure distribution on the spool surface; (2) pressure distribution on the cone surface

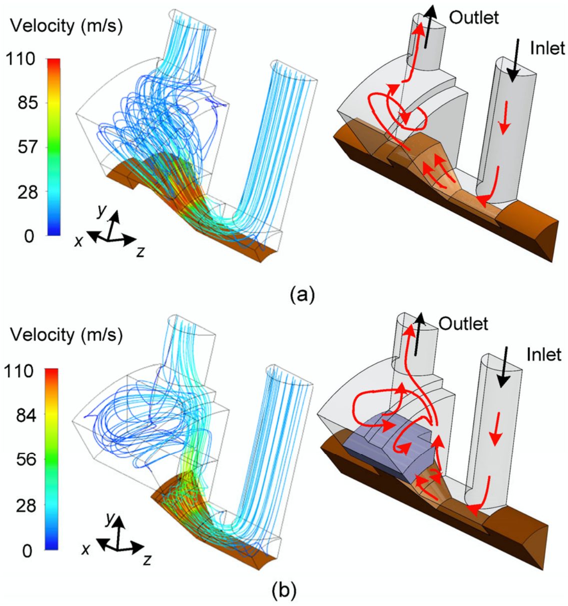

Fig. 10 CFD simulation of the flow structures

(a) Without damping sleeve; (b) With damping sleeve

spool cone surface in the chamber 3 (Fig. 5c). Then, the jet stream is restrained by the damping sleeve orifices and is more perpendicular to the x axis compared to that in the seat valve without the damping sleeve (Fig. 10a). Therefore, the reduction in the jet angle also leads to the decrease of the steady axial flow forces. After the stream hits the 1st sleeve, the fluid particles form swirling vortices angled to the x-y plane. The flow finally gets out after being throttled by the edge of the outlet port.

5.1 Effects of the orifice width *w*

The correlations of the flow forces and the damping orifice width w are analyzed by CFD simulation. The results are verified by the experiments presented in Section 4 and the comparison between the simulated results and experimental results is shown in Fig. 6. The $-x$ direction is chosen as the positive force direction. The simulated and the experimental flow forces show a fairly decreasing linear trend with the increase of the damping orifice width. It is reasonable to see that the CFD results are larger than the experimental ones since the pipe friction loss and pipe fitting loss which the flow experiences are not considered in the numerical computation. The uncertainty (machining errors) of the valves and the damping sleeve also affects the results. As presented in Fig. 6, the flow forces first decrease when the damping orifice width is less than 5 mm. Then they reverse direction when the damping orifice width is 5 mm, and increase in the $-x$ direction with the increment of the width. The flow forces in the $+x$ direction act in the same direction as the actuation force and affect the stability of the seat valve. However, the reduction of the flow forces can be quite significant when the damping sleeve is used.

The damping sleeve acts as a barrier of the flow and influences the flow rate, so the flow reduction needs to be analyzed. The flow loss coefficient δ is defined to describe the flow loss compared to the original valve as

$$\delta = \frac{q_{v1} - q_{v2}}{q_{v1}}, \tag{7}$$

where q_{v1} and q_{v2} represent the flow rates of the valves without and with the damping sleeve, respectively.

The simulated and experimental results are shown in Fig. 11. Both experimental and simulated results show a fairly decreasing trend with the increment of the damping orifice width. The experimental results are larger than the simulated ones since they lack consideration of the test system losses. The system losses affect not only the pressure distribution in the tested valve but also the flow allocation between the tested valve and the relief valve. Therefore, the flow in the experimental environment is more sensitive with the structure of the valve than the simulated flow in the numerical simulation. Therefore, the simulated and the experimental values in this study are still in a fair agreement according to the literature (Aung et al., 2014). Since the five models simulated above fit the experimental results well, the cavitation and other flow status are analyzed using the CFD simulation method.

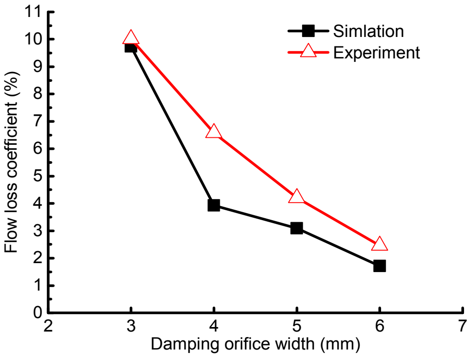

Fig. 11 Flow loss coefficient of different orifice widths

The intensity of the cavitation effects can be observed by CFD simulation. Fig. 12 shows the vapor phase contours of the seat valve without the damping sleeve and the seat valves with different damping orifice widths. Because of the large pressure differential applied on the spool, the cavitation effect is obvious in all conditions. The cavitation appears not only in the narrow restriction region between the spool and the sleeve, but also at the edge of the outlet orifice. The fluid is accelerated in these regions as presented in Fig. 10b.

In the original seat valve (Fig. 12a), the flow is throttled by three metering edges. The flow is accelerated at the spool edge (2nd metering edge) after being throttled by the sharp bend of the 2nd sleeve (1st metering edge) first. However, as shown in Fig. 12b, the effect of the 1st metering edge on the cavitation is changed by the damping sleeve. The damping orifices' edges replace the spool edge and act as the 2nd metering edge. As the width of the damping orifices increase, the cavitation effects strengthen at the 1st metering edge and weaken at the 2nd metering edge. Since the direction of the jet stream is changed by the damping sleeve, the throttling position on the edge of the outlet orifice (3rd metering edge) also changes. The cavitation effect on the 3rd metering edge varies a lot in the valve with the damping sleeve and the valve without the damping sleeve.

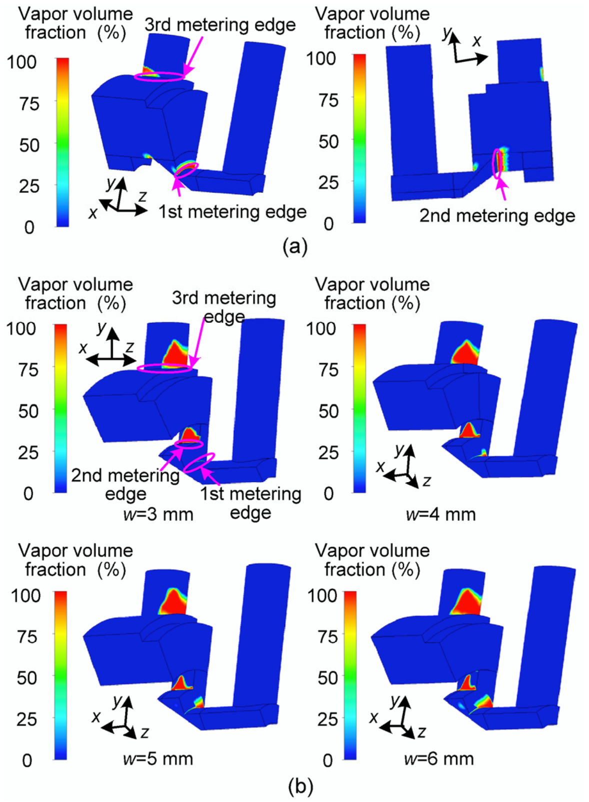

Fig. 12 Vapor volume fraction in the valve chambers
(a) Without damping sleeve; (b) With damping sleeve

However, the cavitation effect changes little with different widths of the damping orifices. To assess cavitation in a more quantitative way, the relative vapor volume σ is used and is calculated by

$$\sigma=\frac{V_{\text{vapor}}}{V}, \tag{8}$$

where V_{vapor} represents the volume of the vapor phase and V indicates the volume of the flow field model. The calculated results are shown in Fig. 13. The cavitation is enhanced by the change of the throttling edges compared with the cavitation in the original valve. With the increase of the orifice width, the weakened throttling function of the damping sleeve increases the cavitation effect.

5.2 Effects of the orifice height *h*

The effects of the orifice height h are studied by simulation. The orifices with the heights of 1.3 mm, 2.0 mm, 2.7 mm, and 3.4 mm and the width of 5 mm at parallel installation position are simulated. The flow forces reduction effects are presented in Fig. 14.

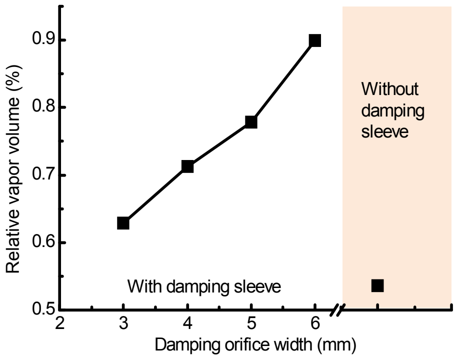

Fig. 13 Relative vapor volume of different orifice widths and the original valve

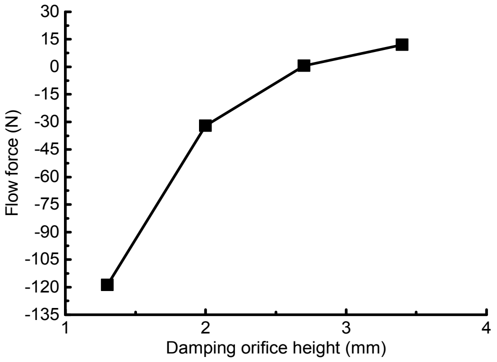

Fig. 14 Flow forces of different orifice heights

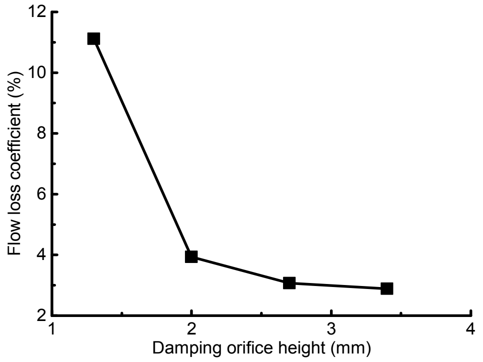

Fig. 15 Flow loss coefficient of different orifice heights

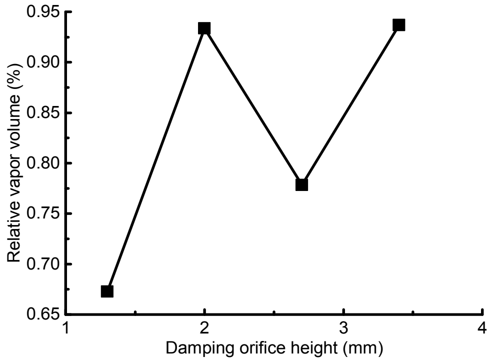

Fig. 16 Relative vapor volume of different orifice heights

The flow forces decrease with the increase of orifice height and reverse direction when the height is 2.7 mm. Then they increase in the opposite direction. The damping orifices with different heights also reduce the flow rate, and the flow loss decreases with the increment of the orifice height, as shown in Fig. 15. Cavitation is also observed in the simulation and the relative vapor volume is presented in Fig. 16. The cavitation effects are also enhanced by using the damping sleeve, but the relative vapor volumes are not monotonic with the change of orifice height. The relative positions of the orifice surfaces and the cone surface of the spool affect the cavitation and the vapor distribution, as presented in Fig. 17.

Fig. 17 shows that the cavitation near the 1st metering edge and the 3rd edge changes little when the orifice height changes. However, as shown in the circles on the right side of Fig. 17, the cavitation effects change a lot near the 2nd metering edge. The orifices' bottom surfaces have a strong impact on the cavitation when the height is 2.0 mm. The effects of the orifices' bottom surfaces on the cavitation weaken while the effects of the orifices' side surfaces strengthen with the increment of orifice height. Therefore, the cavitation is relatively low when the cone edge coincides with orifices' bottom surfaces and the effects of the side surfaces and the bottom surfaces are balanced.

5.3 Effects of relative installation positions

The simulated results on the two limited relative positions between the damping orifices and the outlet ports are depicted in Fig. 18. When the damping orifices are parallel with the outlet ports, as shown in Fig. 18a, the stream flows through the damping orifices and then mainly goes straight to the outlet ports. Part of the flow goes into chamber 4 (Fig. 5c) and forms vortices. However, when the damping orifices are at the angle of 45° to the outlet ports, the entire flow is forced to go through chamber 4 and forms more complex vortices than under the former condition, as shown in Fig. 18b. The generated intenser vortices in chamber 4, which affect the pressure distribution along the spool surface and change the flow forces acting on the spool, dissipate more energy than those in the parallel conditions. The flow

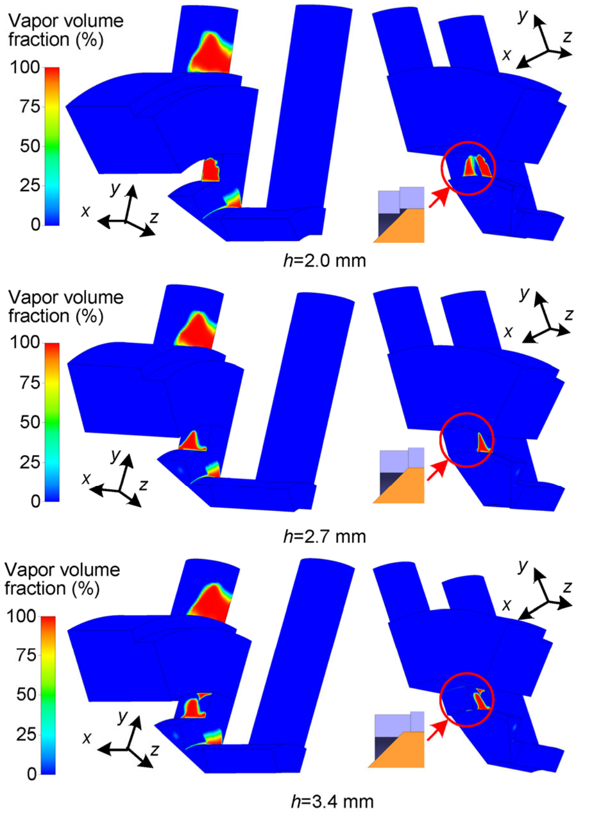

Fig. 17 Vapor volume fraction of different orifice heights

forces under these two conditions are simulated and depicted in Fig. 19.

The flow forces when the damping orifices are at the angle of 45° to the outlet ports show a decreasing trend as in the parallel conditions. The flow forces are about 6 N larger in the +*x* direction as shown in Fig. 19. The additional energy loss reduces the flow capacity of the seat valve, and the flow loss coefficient comparison is shown in Fig. 20. The flow loss coefficients are 0.3%–1.83% larger than those under parallel conditions. It can be seen from the simulation that adjusting the installation angle provides the ability of fine tuning the flow forces with less than 2% flow consumption change.

Fig. 21 presents the relative vapor volume in the simulations. Though the 45° installation reduces the flow capacity of the valve, the cavitation effects are weakened. The cavitation effects in the 45° conditions increase with the increment of the damping orifice width in the same trend as the effects in the parallel conditions. However, compared with the simulated result of the original valve, the cavitation effects can be reduced significantly in the 45° conditions.

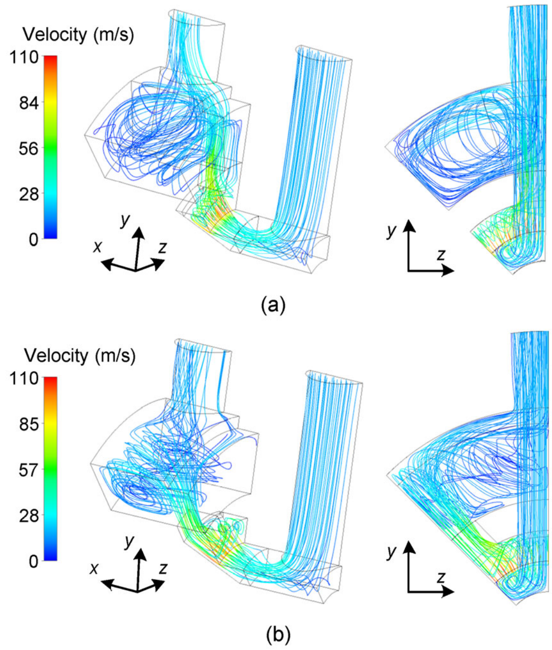

Fig. 18 Streamlines in the valve chambers at parallel and 45° installation positions

(a) Streamlines when damping orifices are parallel with outlet ports; (b) Streamlines when damping orifices are at the angle of 45° to the outlet ports

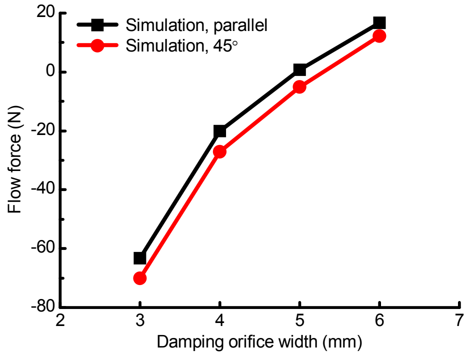

Fig. 19 Flow forces at parallel and 45° installation positions

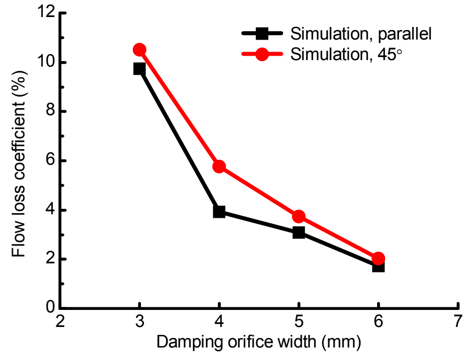

Fig. 20 Flow loss coefficients at parallel and 45° installation positions

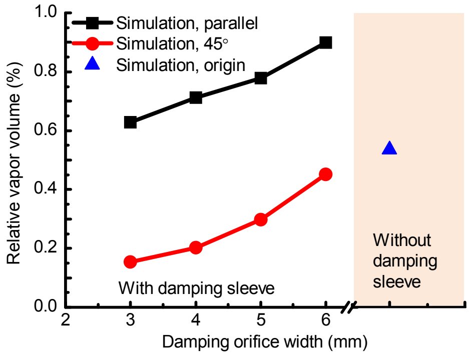

Fig. 21 Relative vapor volume at parallel and 45° installation positions

Simulated and experimental results show that the axial flow forces can be reduced and the direction can also be reversed by applying the damping sleeve. The damping orifice width *w* and height *h* are chosen to be 5 mm and 2.7 mm as the final parameters and the parallel position is chosen as the installation position to assess the effectiveness of the damping sleeve in shortening the valve opening time. The flow forces are reduced from 61.29 N to 1.88 N with 4% flow loss under this condition.

The test rig for simulating the injection system was built and the schematic is presented in Fig. 22. The tested valve is a three-way valve in which the designed damping sleeve is installed to throttle the pressured oil. The spool is connected to the armature and is driven by the electromagnet. The pressured oil is given to a hydraulic transformer to compress the fuel when the valve is opened to the pressure port. When the fuel pressure is high enough, the fuel is jetted back to the fuel tank. When the valve is opened to the tank port, the back pressure in the hydraulic transformer decreases and the fuel is sucked into the hydraulic transformer through the pipes and the check valve using the installed spring. The displacement of the spool is measured with an eddy-current displacement sensor which has the linearity of 1% and the range of 2 mm. In the experiments, the stroke is limited to 0.5 mm by the electromagnet and the armature. The opening time of the valves with and without the damping sleeve is presented in Fig. 23.

When the signal is given to the electromagnet, the electromagnetic force increases and compensates the friction forces and the spring preload. When the electromagnetic force is large enough, the spool moves to open the valve. The spool stops moving when the armature reaches its stroke. As presented in Fig. 23, the opening time of the valve is reduced by 31% from 0.97 ms to 0.67 ms when the damping sleeve is used. The progress in shortening the opening time can help increasing the power density of the free piston engine.

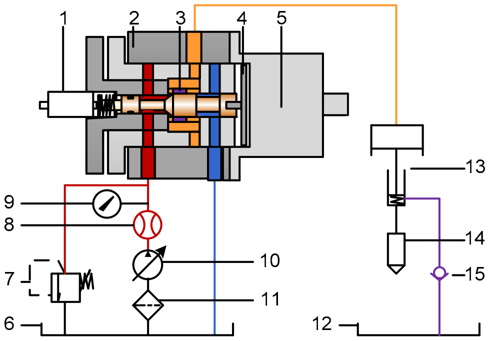

Fig. 22 Schematic of the test rig for the fuel injection system

1-displacement sensor; 2-teseted valve; 3-damping sleeve; 4-armature; 5-electromagnet; 6-hydraulic oil tank; 7-relief valve; 8-flow sensor; 9-pressure sensor; 10-pump; 11-filter; 12-fuel tank; 13-pressure transformer; 14-injector; 15-check valve

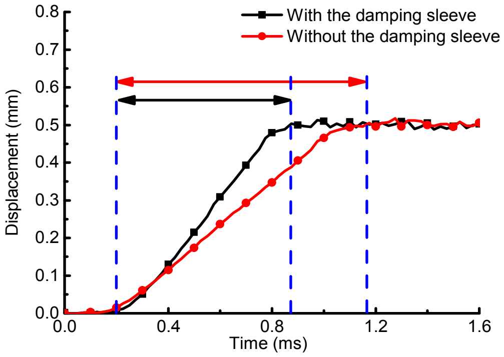

Fig. 23 Comparison of the spool displacements

For further improvement on the power density and reduction on the cavitation, a method will be tried using the 45° relative installation position in practice. Slopes will be processed on the damping sleeve to avoid abrupt throttling of the flow. A pressured fuel supply system will also be built to increase the return pressure of the valve and raise the effectiveness of sucking the fuel.

6 Conclusions

The flow forces reduce the valve opening and slow down the response significantly in the free piston engine, so CFD analysis and experiments are constructed to achieve a good understanding on the flow forces and the flow field. The model is built using a 3D mesh and is refined near the wall. The RNG k-ε model is used to analyze the turbulent flow and the Schnerr and Sauer model is used to simulate the cavitation. The simulated results are validated by experiment.

A damping sleeve with orifices is proposed to reduce the axial flow forces acting on the spool of the seat valve. The effects of the damping orifices with different widths, different heights, and different relative installation positions between the damping sleeve and the outlet ports are analyzed and compared. The pressure distribution along the spool and the jet direction are found in the simulation to be altered by the damping sleeve. The proposed damping sleeve is verified to be able to reduce flow forces and reverse the force direction. The flow loss occurs because of the resistance of the damping sleeve. Since the valve stability is affected by the direction of the flow forces, the damping orifice with a width of 5 mm and height of 2.7 mm at the parallel installation position from the simulated structures is tested in the injection simulation system and the flow forces are reduced from 61.29 N to 1.88 N with 4% flow loss. Based on the laboratory tests of the fuel injection system, the opening time of the valve is reduced by 31% from 0.97 ms to 0.67 ms.

The cavitation effect is observed and needs to be considered to achieve correct flow structure in the simulation. Compared with the cavitation in the original valve, it is enhanced by the parallel installed damping sleeve, and is weakened by the 45° installed damping sleeve. The cavitation also changes when the orifice shape alters, but it cannot be eliminated using the current valve structure or the fuel supply system.

Further research will be oriented towards cavitation optimization by the overall geometrical modifications and injection system improvements. The electromagnet capability should also be improved.

References

Amirante R, Vescovo GD, Lippolis A, 2006. Evaluation of the flow forces on an open centre directional control valve by means of a computational fluid dynamic analysis. *Energy Conversion and Management*, 47(13-14):1748-1760. https://doi.org/10.1016/j.enconman.2005.10.005

Amirante R, Catalano LA, Poloni C, et al., 2014a. Fluid-dynamic design optimization of hydraulic proportional directional valves. *Engineering Optimization*, 46(10): 1295-1314. https://doi.org/10.1080/0305215X.2013.836638

Amirante R, Catalano LA, Tamburrano P, 2014b. The importance of a full 3D fluid dynamic analysis to evaluate the flow forces in a hydraulic directional proportional valve. *Engineering Computations*, 31(5):898-922. https://doi.org/10.1108/EC-09-2012-0221

ANSYS, 2013a. ANSYS/Fluent: Theory Guide, Release 15.0. Swanson Analysis Systems Inc., Houston, USA.

ANSYS, 2013b. ANSYS/Fluent: Users Guide, Release 15.0. Swanson Analysis Systems Inc., Houston, USA.

Aung NZ, Yang QJ, Chen M, et al., 2014. CFD analysis of flow forces and energy loss characteristics in a flapper—nozzle pilot valve with different null clearances. *Energy Conversion and Management*, 83:284-295. https://doi.org/10.1016/j.enconman.2014.03.076

Aung NZ, Peng JH, Li SJ, 2015. Reducing the steady flow force acting on the spool by using a simple jet-guiding groove. International Conference on Fluid Power and Mechatronics, p.289-294. https://doi.org/10.1109/fpm.2015.7337127

Benzon D, Židonis A, Panagiotopoulos A, et al., 2015. Numerical investigation of the spear valve configuration on the performance of Pelton and Turgo turbine injectors and runners. *Journal of Fluids Engineering*, 137(11):111201. https://doi.org/10.1115/1.4030628

Bergada JM, Watton J, 2004. A direct solution for flowrate and force along a cone-seated poppet valve for laminar flow conditions. *Proceedings of the Institution of Mechanical Engineers, Part I: Journal of Systems and Control Engineering*, 218(3):197-210. https://doi.org/10.1177/095965180421800304

Beune A, Kuerten JGM, van Heumen MPC, 2012. CFD analysis with fluid—structure interaction of opening high-pressure safety valves. *Computers & Fluids*, 64:108-116. https://doi.org/10.1016/j.compfluid.2012.05.010

Borghi M, Milani M, Paoluzzi R, 2000. Stationary axial flow force analysis on compensated spool valves. *International Journal of Fluid Power*, 1(1):17-25. https://doi.org/10.1080/14399776.2000.10781079

Borghi M, Milani M, Paltrinieri F, 2004. The effect of flow forces compensating profile on the metering characteristics of a conical seat valve. SAE Commercial Vehicle Engineering Congress and Exhibition, 2004-01-2618. https://doi.org/10.4271/2004-01-2618

Chattopadhyay H, Kundu A, Saha BK, et al., 2012. Analysis of flow structure inside a spool type pressure regulating valve. *Energy Conversion and Management*, 53(1):196-204. https://doi.org/10.1016/j.enconman.2011.08.021

Cheng M, Xu B, Zhang JH, et al., 2017. Valve-based compensation for controllability improvement of the energy-saving electrohydraulic flow matching system. *Journal of Zhejiang University-SCIENCE A (Applied Physics & Engineering)*, 18(6):430-442.

https://doi.org/10.1631/jzus.A1600346

Hu JB, Wu W, Wu MX, et al., 2014. Numerical investigation of the air–oil two-phase flow inside an oil-jet lubricated ball bearing. *International Journal of Heat and Mass Transfer*, 68:85-93. https://doi.org/10.1016/j.ijheatmasstransfer.2013.09.013

Ji C, Lin FY, Zou J, 2017. Experimental investigation of vortex-ring cavitation. *Journal of Zhejiang University-SCIENCE A (Applied Physics & Engineering)*, 18(7): 545-552. https://doi.org/10.1631/jzus.A1600537

Jin ZJ, Wei L, Chen LL, et al., 2013. Numerical simulation and structure improvement of double throttling in a high parameter pressure reducing valve. *Journal of Zhejiang University-SCIENCE A (Applied Physics & Engineering)*, 14(2):137-146. https://doi.org/10.1631/jzus.A1200146

Johnston DN, Edge KA, Vaughan ND, 1991. Experimental investigation of flow and force characteristics of hydraulic poppet and disc valves. *Proceedings of the Institution of Mechanical Engineers, Part A: Journal of Power and Energy*, 205(3):161-171. https://doi.org/10.1243/PIME_PROC_1991_205_025_02

Li K, Sadighi A, Sun ZX, 2014. Active motion control of a hydraulic free piston engine. *IEEE/ASME Transactions on Mechatronics*, 19(4):1148-1159. https://doi.org/10.1109/TMECH.2013.2276102

Li K, Zhang C, Sun ZX, 2015. Precise piston trajectory control for a free piston engine. *Control Engineering Practice*, 34:30-38. https://doi.org/10.1016/j.conengprac.2014.09.016

Li SJ, Aung NZ, Zhang SZ, et al., 2013. Experimental and numerical investigation of cavitation phenomenon in flapper–nozzle pilot stage of an electrohydraulic servovalve. *Computers & Fluids*, 88:590-598. https://doi.org/10.1016/j.compfluid.2013.10.016

Martins NMC, Soares AK, Ramos HM, et al., 2016. CFD modeling of transient flow in pressurized pipes. *Computers & Fluids*, 126:129-140. https://doi.org/10.1016/j.compfluid.2015.12.002

Merritt HE, 1967. Hydraulic Control Systems. John Wiley & Sons, New York, USA, p.25-53.

Reichert M, 2010. Development of High-response Piezoservovalves for Improved Performance of Electrohydraulic Cylinder Drives. PhD Thesis, RWTH Aachen University, Aachen, Germany.

Saha BK, Chattopadhyay H, Mandal PB, et al., 2014. Dynamic simulation of a pressure regulating and shut-off valve. *Computers & Fluids*, 101:233-240. https://doi.org/10.1016/j.compfluid.2014.06.011

Shojaeefard MH, Tahani M, Ehghaghi MB, et al., 2012. Numerical study of the effects of some geometric characteristics of a centrifugal pump impeller that pumps a viscous fluid. *Computers & Fluids*, 60:61-70. https://doi.org/10.1016/j.compfluid.2012.02.028

Simic M, Herakovic N, 2015. Reduction of the flow forces in a small hydraulic seat valve as alternative approach to improve the valve characteristics. *Energy Conversion and Management*, 89:708-718. https://doi.org/10.1016/j.enconman.2014.10.037

Valdés JR, Rodríguez JM, Monge R, et al., 2014. Numerical simulation and experimental validation of the cavitating flow through a ball check valve. *Energy Conversion and Management*, 78:776-786. https://doi.org/10.1016/j.enconman.2013.11.038

Wu W, Xiong Z, Hu JB, et al., 2015. Application of CFD to model oil-air flow in a grooved two-disc system. *International Journal of Heat and Mass Transfer*, 91:293-301. https://doi.org/10.1016/j.ijheatmasstransfer.2015.07.092

Yakhot V, Orszag SA, 1986. Renormalization group analysis of turbulence. I. Basic theory. *Journal of Scientific Computing*, 1(1):3-51. https://doi.org/10.1007/BF01061452

Zhang SL, Zhao ZF, Zhao CL, et al., 2016. Experimental study of hydraulic electronic unit injector in a hydraulic free piston engine. *Applied Energy*, 179:888-898. https://doi.org/10.1016/j.apenergy.2016.07.051

中文概要

题　目：使用带孔阻尼套的座阀液动力试验和数值研究

目　的：液压自由活塞发动机性能受燃油喷射系统开关阀性能限制。本文旨在对开关阀内部结构进行优化，降低液动力，从而提高阀的开启速度。

创新点：1. 提出一种易于安装的带孔阻尼套结构，可以用于改变阀芯表面压力分布和油液射流角，从而降低液动力；2. 建立数值仿真模型，分析阻尼套不同结构和安装参数对液动力和空化的影响。

方　法：1. 进行数值模拟，分析阀芯表面压力分布和内部流场分布，并通过实验验证方法有效性和模型准确性；2. 对不同阻尼孔宽度、深度和相对位置下的阀芯液动力和流量损失情况进行对比和分析；3. 对上述不同阻尼孔结构下阀内空化情况进行仿真和对比；4. 建立燃油喷射系统试验台，验证阻尼套对提高阀开启速度的作用。

结　论：1. 提出的带孔阻尼套结构可以有效降低阀芯液动力。2. 随阻尼孔的减小，其对液动力的改变作用和节流作用逐渐增强；阻尼孔足够小时液动力反向并逐渐加强。3. 阻尼套对油液的阻碍作用也会改变流场内的空化情况，但空化强度不一定随节流孔的变大而单调变强，其还受相对安装位置影响。4. 带孔阻尼套可以有效降低阀的开启时间。

关键词：座阀；阻尼套；液动力；数值研究